



## Preparation, characterization of nanocomposites plasmonic photocatalyst C@( $\text{Fe}_3\text{O}_4$ -halloysite nanotubes)-Ag/AgCl and its photocatalytic activity

Yu-bin Tang<sup>a,b,\*</sup>, Hu-jun Yang<sup>a</sup>, Fang-yan Chen<sup>a</sup>, Xin-gang Wang<sup>a</sup>

<sup>a</sup>School of Environmental and Chemical Engineering, Jiangsu University of Science and Technology, Zhenjiang Jiangsu, 212003, China

<sup>b</sup>Institute of Industrial Technology, Jiangsu University of Science and Technology, Zhangjiagang, 215600, China,

Tel. +86 511 84448601; email: ybbill@163.com (Y.-b. Tang), Tel. +86 511 85605157; emails: 825623025@qq.com (H.-j. Yang), catchen1029@sohu.com (F.-y. Chen), hofs@163.com (X.-g. Wang)

Received 8 October 2017; Accepted 16 March 2018

### ABSTRACT

The work reports the fabrication of C@( $\text{Fe}_3\text{O}_4$ -halloysite nanotubes)-Ag/AgCl by growing Ag/AgCl on the surface of the carbonization of halloysite nanotubes (hereinafter referred to as HNT<sub>s</sub>) supported ferroferric oxide hybrid via precipitation-photoreduction method. The structural characteristics of the resulting composite catalyst were studied with X-ray powder diffraction, SEM-energy dispersive X-ray spectroscopy, X-ray photoemission spectroscopy, Fourier transform infrared spectroscopy and UV-Vis diffuse reflectance spectra; the photocatalytic performance of the resulted catalysts were tested using methyl orange (MO) as a model contaminant under visible light irradiation ( $\lambda > 400$  nm). The C@( $\text{Fe}_3\text{O}_4$ -HNT<sub>s</sub>)-Ag/AgCl composites with 5 wt% C@( $\text{Fe}_3\text{O}_4$ -HNT<sub>s</sub>) showed the highest photocatalytic activity, degrading 97.71% MO after 40 min irradiation and maintaining the high activity even after five cycles. Except for the high removal efficiency of MO, remarkable  $\cdot\text{O}_2^-$  generation performance, and good stability of C@( $\text{Fe}_3\text{O}_4$ -HNT<sub>s</sub>)-Ag/AgCl could be attributed to the presence of carbon-containing organic group and  $\text{Fe}^{3+}$  as well, which can act as an electron acceptor for photo-induced electrons from Ag/AgCl during the photocatalytic process and then inhibit the photocorrosion.

*Keywords:* Halloysite nanotubes; Ag/AgCl;  $\text{Fe}_3\text{O}_4$ ; Composite; Photocatalytic activity

### 1. Introduction

Photocatalytic technology, which can utilize solar energy as direct driving force, has obvious advantages and potential application value in solving the problem of energy shortage and environmental pollution, is one of the hot research topic in the field of environmental purification. The basis on which photocatalytic technology plays a role in the two fields mentioned above is preparation of efficient photocatalytic materials. However, traditional photocatalyst  $\text{TiO}_2$  with large band gap (3.0–3.2 eV) can only absorb UV light and restricts its wide practical applications in the case of natural solar light, hence exploiting visible-light-driven photocatalyst is the key to utilize solar energy efficiently. Except for anion

doping, cation doping, co-doping, crystal facets control, heterojunction fabrication and surface amorphization, as a novel approach to improve the visible-light-driven photocatalytic performance, plasmonic photocatalyst which can combine the advantages of both surface plasmon resonance (SPR) and photocatalysis has attracted more attention since it was first reported in 2008 [1].

As a general rule, plasmonic photocatalysts include noble metal (such as Ag, Au and Pt) and semiconductor (such as Ag/AgCl, Ag/AgBr and Ag/AgI) [2]. It has been reported that silver-silver halide composite nano-photocatalysts with visible light response and SPR can be used for the degradation of pollutants [3]. Silver-based photocatalyst is widely used to study the degradation of organic pollutants in water, photocatalytic hydrogen production and chemical synthesis [4–6]. Tian et al. [7] reported that the main factor affecting the photostability of Ag/AgCl was the content of

\* Corresponding author.

Ag<sup>0</sup> nanoclusters. Studies have also shown that oxidizability of Cl<sup>-</sup> generated by silver-based catalysts Ag/AgX (X = Cl, Br) in the photocatalytic reaction process is better than that of Br<sup>-</sup> and I<sup>-</sup> [8]. However, Ag/AgCl also suffers from a high recombination rate of photogenerated electron-hole pairs and photocorrosion in the photocatalytic process, which greatly inhibit their practical applications. As AgCl is reduced to Ag<sup>0</sup>, the content of AgCl is relatively lowered, which, in turn, will inhibit the generation rate of holes and Cl<sup>-</sup> [9]. In order to solve this problem, the silver/silver halide photocatalyst is deposited on the surface of the semiconductor photocatalyst, and the composites photocatalysts with heterojunction is prepared, which can accelerate the transfer of photo-generated electrons, inhibit the recombination of photo-generated electron-holes pairs and the photocorrosion of the photocatalysts [10], and noble metal nanoclusters can form Schottky junctions with semiconductor photocatalysts to enhance photocatalytic property of composites [11]. Liu et al. [12] prepared an Ag@AgCl/Cu<sub>2</sub>O composite photocatalyst by directly growing Ag@AgCl nanoparticles on (111) facets of octahedral Cu<sub>2</sub>O via a facile precipitation in situ photoreduction method, which can effectively inhibit the recombination of photo-generated electron-hole pairs. The separation and reclamation of Ag/AgCl particles are crucial for their further applications. Moreover, Li et al. [13] and Dong et al. [14] synthesized AgX-SmVO<sub>4</sub> (X = Br, Cl, I) via deposition method, showed high visible-light photocatalytic activity for the photocatalytic degradation of rhodamine B (RhB) in aqueous solutions. Zhao et al. [15] deposited Ag on Fe<sub>3</sub>O<sub>4</sub>@TiO<sub>2</sub> surface by hydrothermal method to form binary composite photocatalyst. Fe<sub>3</sub>O<sub>4</sub> not only provides more active sites for the formation of ·O<sub>2</sub><sup>-</sup> but also highlights the advantages of the composites for easy separation, and the heterojunction and Fe<sub>3</sub>O<sub>4</sub> cocatalyst in the composite can facilitate the transfer of photogenerated charge carriers. The smaller specific surface area of cubic Ag/AgCl is also the main factor restricting its photocatalytic activity. Some researchers synthesized Ag/AgCl/ZnO [16], Ag/AgCl/SiO<sub>2</sub> [17], Ag/AgBr/TiO<sub>2</sub> [18], flower-like Ag@AgCl/Bi<sub>2</sub>WO<sub>6</sub> [19], K<sub>4</sub>Nb<sub>6</sub>O<sub>17</sub>/Ag@AgBr [20] and other composites photocatalysts. When Ag/AgCl is dispersed on these materials (such as SiO<sub>2</sub> and ZnO), they become much smaller in size, therefore the specific surface area and active site of the composites increased. The Ag/AgX of smaller particles favors the transfer of photogenerated carriers and reduces the recombination rate of photogenerated electron-hole pairs [21]. So, it is the main approach to promote the application of Ag/AgCl plasmonic photocatalysts by suppressing the recombination of photogenerated electron-hole pairs, enhancing its separation performance and increasing its specific surface area. Song et al. [22] studied the photocatalytic activity of CS-Ag<sub>3</sub>PO<sub>4</sub>. The results showed that the interfacial effect of C-microspheres and Ag<sub>3</sub>PO<sub>4</sub> contribute to improving the photoactivity. Z-Scheme AgI/Bi<sub>5</sub>O<sub>7</sub>I hybrid and AgBr/Bi<sub>3</sub>O<sub>4</sub>Br hybrid were successfully prepared via a simple one-step ionic reaction, AgI particles are closely anchored on Bi<sub>5</sub>O<sub>7</sub>I micro rods, the interactions between the components are important for the formation of a heterojunction structure in the composite photocatalysts, and this structure contributes to the separation of electron-hole pairs and subsequently results in their high photoactivity [23,24].

Clay materials could be categorized into cationic clays and anionic clays [25], they have specific features such as their nanometer-scale layers and interlayers and their capacity for versatile tuning of the components on layers and within interlayers, so they are very suitable to be designed and transformed into function materials. In recent decades, clay materials have been widely used as adsorbents for the enrichment of organic pollutants and heavy metal ions because of their special layered structure, large specific surface area and good adsorption performance. Xu et al. [26] synthesized Ag<sub>3</sub>PO<sub>4</sub>/Fe-Al/Mt composites photocatalyst by loading Ag<sub>3</sub>PO<sub>4</sub> on hydroxyl-iron-aluminum pillared montmorillonite (Fe-Al/Mt), in which Fe<sup>3+</sup> worked as an active site for the following oxygen reduction to reduce the recombination rate of photogenerated e<sup>-</sup>h<sup>+</sup>, accelerate the transfer of photogenerated carriers and prevent the photocorrosion of Ag<sub>3</sub>PO<sub>4</sub>. Liu and Zhang [25] proposed that clay materials as carriers for photocatalysts have two advantages: first, good adsorption performance and the hydrophilic group on the surface favor to enrich dye molecules and accelerate the photocatalytic reaction rate; second, some clay materials can directly participate in the photochemical reaction by their functional groups, improve the separation of electron and hole pairs, thereby enhancing the photocatalytic activity and photostability.

In the present paper, halloysite nanotubes (HNT<sub>s</sub>) were selected as the pore-forming agent to increase the specific surface area of Ag/AgCl. The carbon-containing functional groups were grafted on the surface of HNT<sub>s</sub> to improve the performance of photoexcited electron trapping. The prepared composites material C@(Fe<sub>3</sub>O<sub>4</sub>-HNT<sub>s</sub>) was used as cocatalyst to accelerate the transfer of photogenerated charge carriers. Finally, composites plasmonic photocatalyst C@(Fe<sub>3</sub>O<sub>4</sub>-HNT<sub>s</sub>)-Ag/AgCl was synthesized by the "three-step method". This work provides a new material and theoretical reference for the photocatalytic degradation of organic substances such as azo dyes.

## 2. Experimental section

### 2.1. Materials

Hexahydrate ferric chloride, ethylene glycol, sodium acetate trihydrate, polyethylene glycol, glucose, anhydrous ethanol, silver nitrate and sodium chloride were all purchased from Sinopharm Group Chemical Reagent Co., Ltd. (Shanghai China). HNT<sub>s</sub> were purchased from Yatong Mineral Powder Factory, Hebei Province, China.

All the chemicals used were of analytical grade. Deionized water was used throughout the experiments.

### 2.2. Preparation of Fe<sub>3</sub>O<sub>4</sub>-HNT<sub>s</sub>

A typical preparation method of Fe<sub>3</sub>O<sub>4</sub>-HNT<sub>s</sub> composites was as follows:

Accurately weigh 1.08 g of FeCl<sub>3</sub>·6H<sub>2</sub>O and dissolve it in a beaker filled with 80 mL ethylene glycol (EG) under a magnetic stirring condition to form a stable orange solution, and then immediately add 0.8 g of HNT<sub>s</sub> into the beaker, stirring for 24 h continuously. 5.8963 g of sodium acetate trihydrate (NaAc·3H<sub>2</sub>O) and 1.0 g of polyethylene glycol were then weighed into the aqueous dispersion mentioned above, then

the dispersion was magnetically stirred for 30 min enabling sodium acetate and polyethylene glycol to completely dissolve, forming precursor. The precursor was then sealed in a 100 mL Teflon-lined stainless steel autoclave and heated at 200°C for 8 h, and then cooled down to room temperature. The as-prepared  $\text{Fe}_3\text{O}_4\text{-HNT}_5$  was centrifuged and washed for three times with ethanol and deionized water.

### 2.3. Preparation of $\text{C}@\text{(Fe}_3\text{O}_4\text{-HNT}_5\text{)}$

0.4 g of  $\text{Fe}_3\text{O}_4\text{-HNT}_5$  composites was dispersed in 40 mL of glucose solution (10 g/L) under ultrasonic vibration to form a homogeneous dark suspension at 25°C. The suspension was then sealed in a 100 mL Teflon-lined stainless steel autoclave and maintained at 180°C for 48 h, and then cooled down to room temperature. The as-prepared black product  $\text{C}@\text{(Fe}_3\text{O}_4\text{-HNT}_5\text{)}$  was rinsed for five times with ethanol and then centrifuged followed by washing for three times with ultrapure water, finally, dried at 70°C for 12 h under vacuum.

### 2.4. Synthesis of $\text{C}@\text{(Fe}_3\text{O}_4\text{-HNT}_5\text{)-Ag/AgCl}$

1 wt%  $\text{C}@\text{(Fe}_3\text{O}_4\text{-HNT}_5\text{)-Ag/AgCl}$  composites were prepared by precipitation–photoreduction method.

In a typical process, 7.24 mg of  $\text{C}@\text{(Fe}_3\text{O}_4\text{-HNT}_5\text{)}$  was dispersed in 200 mL deionized water to form suspension A. 0.85 g of  $\text{AgNO}_3$  was weighed and added into suspension A, then, agitated for 2 h at a dark condition. 25 mL of NaCl aqueous solution (0.2 M) was added dropwise into the suspension A successively within 30 min under mechanical stirring. The vigorous stirring was maintained for 24 h at room temperature to form homogeneous suspension. And then, the suspension was irradiated with a 500 W xenon arc lamp for 15 min. Then, the resulting precipitate was separated and washed with deionized water and dried under 80°C for 12 h. The products were named as 1 wt%  $\text{C}@\text{(Fe}_3\text{O}_4\text{-HNT}_5\text{)-Ag/AgCl}$ .

As mentioned above, four photocatalysts with different mass fraction of  $\text{C}@\text{(Fe}_3\text{O}_4\text{-HNT}_5\text{)}$  were prepared, which refer to 1 wt%  $\text{C}@\text{(Fe}_3\text{O}_4\text{-HNT}_5\text{)-Ag/AgCl}$ , 5 wt%  $\text{C}@\text{(Fe}_3\text{O}_4\text{-HNT}_5\text{)-Ag/AgCl}$ , 10 wt%  $\text{C}@\text{(Fe}_3\text{O}_4\text{-HNT}_5\text{)-Ag/AgCl}$ , and 15 wt%  $\text{C}@\text{(Fe}_3\text{O}_4\text{-HNT}_5\text{)-Ag/AgCl}$ . When the mass percentage of the composite  $\text{C}@\text{(Fe}_3\text{O}_4\text{-HNT}_5\text{)}$  introduced to plasmonic photocatalyst  $\text{C}@\text{(Fe}_3\text{O}_4\text{-HNT}_5\text{)-Ag/AgCl}$  was 1 wt%, the sample was named as 1 wt%  $\text{C}@\text{(Fe}_3\text{O}_4\text{-HNT}_5\text{)-Ag/AgCl}$ , and so forth.

The pure Ag/AgCl was prepared using a similar method mentioned above without the addition of  $\text{C}@\text{(Fe}_3\text{O}_4\text{-HNT}_5\text{)}$ . Other mass ratios of  $\text{C}@\text{(Fe}_3\text{O}_4\text{-HNT}_5\text{)-Ag/AgCl}$  were obtained by adding different mass of  $\text{C}@\text{(Fe}_3\text{O}_4\text{-HNT}_5\text{)}$ . Note that the washing works mentioned above were performed without protection from the ambient light.

### 2.5. Characterization

The infrared spectra of  $\text{C}@\text{(Fe}_3\text{O}_4\text{-HNT}_5\text{)}$  and  $\text{HNT}_5$  were determined by TENSOR 27 Fourier transform infrared spectroscopy (FTIR) by diffuse reflectance scanning technique from 4,000 to 400  $\text{cm}^{-1}$ . The UV–Vis absorption spectra of  $\text{C}@\text{(Fe}_3\text{O}_4\text{-HNT}_5\text{)-Ag/AgCl}$  in solid state were obtained using a UV–Vis spectrophotometer (UV-2550, Shimadzu Corporation, Japan). The morphology and structure of the

products were studied by transmission electron microscope (TEM: Tecnai 12, Philips company, Holland) equipped with an energy dispersive X-ray spectroscope (EDS) running at an acceleration voltage of 10 kV. The crystalline phases of prepared materials were studied by X-ray diffractometer (D8 Advance system, Germany Bruker group, Karlsruhe) with Cu K $\alpha$  radiation ( $\lambda = 1.54 \text{ \AA}$ ) in the  $2\theta$  range of 10°–80°. X-ray photoemission spectroscopy (XPS) was measured on a PHI5300 with a monochromatic Mg K $\alpha$  source.

### 2.6. Photocatalytic performance test of $\text{C}@\text{(Fe}_3\text{O}_4\text{-HNT}_5\text{)-Ag/AgCl}$

Photocatalytic activities of composite  $\text{C}@\text{(Fe}_3\text{O}_4\text{-HNT}_5\text{)-Ag/AgCl}$  were evaluated by methyl orange (MO) degradation experiments under visible light irradiation, which was provided by a 300 W Xe lamp with  $\lambda > 400 \text{ nm}$  and light intensity of 60  $\text{mW/cm}^2$ .

In a typical photocatalytic degradation experiment, 50 mg of photocatalyst prepared was dispersed in 100 mL of MO aqueous solution with initial concentration of 10 mg/L. Then the suspension was first stirred for 0.5 h in the dark to ensure adsorption/desorption equilibrium between photocatalysts and MO, and then the lamp was lit to start irradiation. 4 mL of suspension was sampled per 10 min and centrifuged completely to remove all of the powder. After that, MO concentrations of the supernatant were monitored by recording the maximum absorption band (465 nm for MO). The degradation rate was calculated as following formula:

$$E = \frac{A_0 - A_t}{A_0} \times 100\% \quad (1)$$

where  $A_0$  is primal MO absorbance,  $A_t$  is time-dependent MO absorbance upon irradiation.

## 3. Results and discussion

### 3.1. Characterization

#### 3.1.1. TEM–EDS analysis of the materials

TEM images of the samples are shown in Fig. 1. Fig. 1(a) is transmission electron micrograph of  $\text{HNT}_5$ . It can be seen from Fig. 1(a),  $\text{HNT}_5$  appear a hollow tubular structure, the tube length distribution is inhomogeneous, the longer one is about 800 nm long, the tube wall is thinner and about 10 nm. In addition, the halloysite tubes have external diameters of about 50–60 nm and inner diameters of about 10–20 nm, which is identical to those of previously reported samples. Fig. 1(b) is transmission electron micrograph of the cocatalyst  $\text{C}@\text{(Fe}_3\text{O}_4\text{-HNT}_5\text{)}$ . It can be seen from Fig. 1(b) that  $\text{Fe}_3\text{O}_4$  nanospheres were synthesized by ethylene glycol solvothermal method [27], with an average diameter of 20 nm. After hydrothermal treatment, the  $\text{Fe}_3\text{O}_4\text{-HNT}_5$  was covered with a layer of organic molecules, in this research;  $\text{Fe}_3\text{O}_4\text{-HNT}_5$  acted as template for the deposition of organic molecules, the presence of templates in hydrothermal carbonization process could effectively prevent the homogeneous nucleation of carbon species and promote the homogeneous deposition of carbonaceous matter on the external of templates.

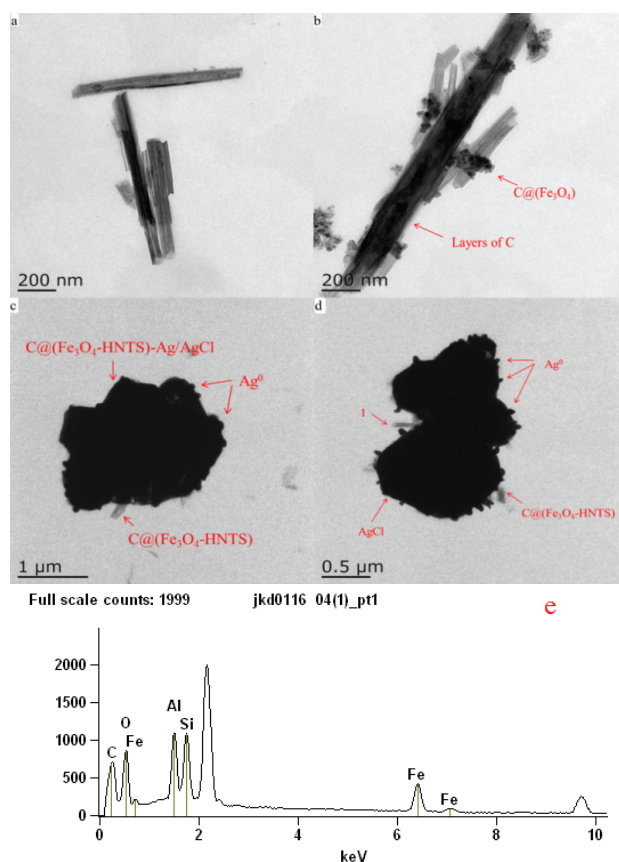


Fig. 1. TEM image of HNT<sub>5</sub> (a), C@(Fe<sub>3</sub>O<sub>4</sub>-HNT<sub>5</sub>) (b), C@(Fe<sub>3</sub>O<sub>4</sub>-HNT<sub>5</sub>)-Ag/AgCl ((c) and (d)) and EDS of C@(Fe<sub>3</sub>O<sub>4</sub>-HNT<sub>5</sub>) (e).

From Figs. 1(c) and (d), we can see that when C@(Fe<sub>3</sub>O<sub>4</sub>-HNT<sub>5</sub>) was introduced to the Ag/AgCl sample, some holes can be seen on the particles' surface and small amounts of HNT<sub>5</sub> were observed on the surfaces of the samples. The particles on C@(Fe<sub>3</sub>O<sub>4</sub>-HNT<sub>5</sub>)-Ag/AgCl composites surface may be Ag particles with more uniformly distributed and smaller size (10–50 nm).

### 3.1.2. X-ray powder diffraction

The phase structure of the HNT<sub>5</sub>, Fe<sub>3</sub>O<sub>4</sub>, C@(Fe<sub>3</sub>O<sub>4</sub>-HNT<sub>5</sub>), Ag/AgCl and 5 wt% C@(Fe<sub>3</sub>O<sub>4</sub>-HNT<sub>5</sub>)-Ag/AgCl was investigated by X-ray powder diffraction (XRD). A typical XRD pattern of the as-obtained samples are shown in Fig. 2.

The XRD pattern of C@(Fe<sub>3</sub>O<sub>4</sub>-HNT<sub>5</sub>) (Fig. 2(c)) shows a broad peak located at about  $2\theta = 20^\circ$  which can be ascribed to the diffraction of amorphous carbon [28], indicating that glucose molecules were polymerized and carbonized on the surface of Fe<sub>3</sub>O<sub>4</sub>-HNT<sub>5</sub>, the peaks at  $2\theta = 12.57^\circ$ ,  $20.18^\circ$  and  $35.01^\circ$  are assigned, respectively, to the (001), (100) and (002) planes of HNT<sub>5</sub> [29]. By comparing with patterns of HNT<sub>5</sub> (Fig. 2(a)), the peaks of (001), (100) and (002) of the original HNT<sub>5</sub> still existed but became weak and were covered by broad peak of amorphous carbon due to the carbonization of organic materials on the surface of Fe<sub>3</sub>O<sub>4</sub>-HNT<sub>5</sub>.

The diffraction peaks of C@(Fe<sub>3</sub>O<sub>4</sub>-HNT<sub>5</sub>) at  $30.0^\circ$ ,  $35.3^\circ$ ,  $43.18^\circ$ ,  $57.0^\circ$  and  $62.4^\circ$  can be assigned to the (220), (311),

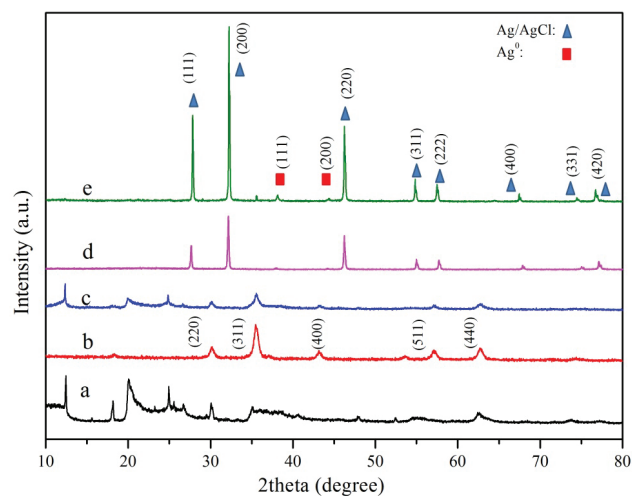


Fig. 2. XRD patterns of HNT<sub>5</sub> (a), Fe<sub>3</sub>O<sub>4</sub> (b), C@(Fe<sub>3</sub>O<sub>4</sub>-HNT<sub>5</sub>) (c), Ag/AgCl (d), 5 wt% C@(Fe<sub>3</sub>O<sub>4</sub>-HNT<sub>5</sub>)-Ag/AgCl (e).

(400), (511) and (440) crystal planes of the pure cubic Fe<sub>3</sub>O<sub>4</sub> (JCPDS card no 19-0629), respectively (Fig. 2, curve c). The XRD peaks of 5 wt% C@(Fe<sub>3</sub>O<sub>4</sub>-HNT<sub>5</sub>)-Ag/AgCl at  $27.8^\circ$ ,  $32.2^\circ$ ,  $46.23^\circ$ ,  $54.82^\circ$ ,  $57.48^\circ$ ,  $67.47^\circ$ ,  $74.47^\circ$  and  $76.73^\circ$  are assigned to the (111), (200), (220), (311), (222), (400), (331) and (420) crystal planes of the cubic phase AgCl (JCPDS card no 31-1238), respectively. The (111) and (200) planes of metallic Ag were observed at  $38.12^\circ$  and  $44.28^\circ$  [12]. The characteristic diffraction peak of Fe<sub>3</sub>O<sub>4</sub> and HNT<sub>5</sub> is not obvious in the XRD of the composites plasmonic photocatalyst C@(Fe<sub>3</sub>O<sub>4</sub>-HNT<sub>5</sub>)-Ag/AgCl, which may be because of the low intensity of C@(Fe<sub>3</sub>O<sub>4</sub>-HNT<sub>5</sub>).

From TEM-EDS and XRD results, it can be inferred that the composite C@(Fe<sub>3</sub>O<sub>4</sub>-HNT<sub>5</sub>)-Ag/AgCl has been prepared.

### 3.1.3. Infrared spectrum analysis

Figs. 3(a)–(d) show FTIR spectra of the 5 wt% C@(Fe<sub>3</sub>O<sub>4</sub>-HNT<sub>5</sub>)-Ag/AgCl, HNT<sub>5</sub>, Ag/AgCl and C@(Fe<sub>3</sub>O<sub>4</sub>-HNT<sub>5</sub>), respectively.

The characteristic bands at  $3,685$  and  $3,619$   $\text{cm}^{-1}$  are due to the Al-OH stretching vibration, the peak at  $1,034$   $\text{cm}^{-1}$  corresponds to the Si-O network (Si-O-Si and O-Si-O) for HNT<sub>5</sub>. And the band at  $912$   $\text{cm}^{-1}$  represents Al-OH bending vibration which is clearly seen in the HNT<sub>5</sub> and C@(Fe<sub>3</sub>O<sub>4</sub>-HNT<sub>5</sub>) samples [30] (see curve b). The bands at  $2,921$ ;  $1,700$  and  $1,625$   $\text{cm}^{-1}$  were attributed to C-H stretching vibration of grafted organic groups, C=O stretching vibrations and C=C bond conjugated with carbonyl, respectively. The weak peaks between  $1,300$  and  $1,450$   $\text{cm}^{-1}$  are assigned to various -CH<sub>2</sub>- stretching vibration modes and O-H in-plane bending vibrations, respectively [29,30] (see curve d).

It can be seen from Fig. 3 that the carbon-containing functional groups such as -COOH, -CH<sub>2</sub>- and C=C are successfully grafted on the surface of Fe<sub>3</sub>O<sub>4</sub>-HNT<sub>5</sub> by hydrothermal method. When the hydrothermal temperature is below  $200^\circ\text{C}$ , glucose could not be completely carbonized but can form a large number of carbon containing functional groups and 5-hydroxymethyl furfural (HMF) on the surface of Fe<sub>3</sub>O<sub>4</sub>-HNT<sub>5</sub> [31,32]. In addition, due to the presence

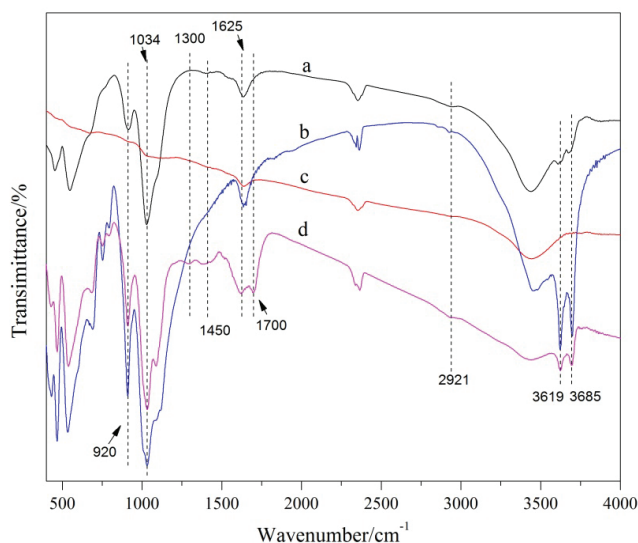


Fig. 3. FTIR spectra of 5 wt% C@(Fe<sub>3</sub>O<sub>4</sub>-HNT<sub>s</sub>)-Ag/AgCl (a), HNT<sub>s</sub> (b), Ag/AgCl (c) and C@(Fe<sub>3</sub>O<sub>4</sub>-HNT<sub>s</sub>) (d).

of cocatalyst C@(Fe<sub>3</sub>O<sub>4</sub>-HNT<sub>s</sub>), the C@(Fe<sub>3</sub>O<sub>4</sub>-HNT<sub>s</sub>)-Ag/AgCl shows new and several characteristic peaks at 3,685; 3,619; 2,921; 1,700; 1,450; 1,300, 1,034 and 920 cm<sup>-1</sup> compared with pure Ag/AgCl. Therefore, nano-materials C@(Fe<sub>3</sub>O<sub>4</sub>-HNT<sub>s</sub>)-Ag/AgCl was confirmed by FTIR results.

### 3.1.4. Diffuse reflectance UV-Vis spectroscopy

The UV-Vis diffuse reflectance spectra of C@(Fe<sub>3</sub>O<sub>4</sub>-HNT<sub>s</sub>), Ag/AgCl and C@(Fe<sub>3</sub>O<sub>4</sub>-HNT<sub>s</sub>)-Ag/AgCl with different C@(Fe<sub>3</sub>O<sub>4</sub>-HNT<sub>s</sub>) content are shown in Fig. 4.

From Fig. 4, we can see, due to the existence of plasmon resonance of Ag NPs, the pure Ag/AgCl and composite C@(Fe<sub>3</sub>O<sub>4</sub>-HNT<sub>s</sub>)-Ag/AgCl exhibits a broad absorption within the visible region (400–800 nm). This is due to the plasma resonance effect (SPR) of Ag nanoparticles [7,33]. The bulging peaks of surface plasmon resonance located around at 480 nm, which is also the function of SPR. When Ag/AgCl nanoparticles were grown on the C@(Fe<sub>3</sub>O<sub>4</sub>-HNT<sub>s</sub>) surface, the absorption efficiency of light (less than 400 nm) of the composite photocatalyst C@(Fe<sub>3</sub>O<sub>4</sub>-HNT<sub>s</sub>)-Ag/AgCl was obviously enhanced. When the content of cocatalyst C@(Fe<sub>3</sub>O<sub>4</sub>-HNT<sub>s</sub>) was more than 5%, the absorption effect of C@(Fe<sub>3</sub>O<sub>4</sub>-HNT<sub>s</sub>)-Ag/AgCl in UV and visible region were both decreased. Compared with Ag/AgCl, the composite photocatalysts with different cocatalyst contents all weaken the absorption effect at 420–550 nm, which is the result of the substitution of C@(Fe<sub>3</sub>O<sub>4</sub>-HNT<sub>s</sub>) for some Ag/AgCl.

### 3.1.5. Elemental compositions

The elemental composition and chemical states of C@(Fe<sub>3</sub>O<sub>4</sub>-HNT<sub>s</sub>)-Ag/AgCl prepared were further investigated by XPS measurements, as displayed in Fig. 5.

The survey XPS spectrum (Fig. 5(a)) confirms the existence of ingredient elements of Fe, O, Ag, Cl, C, Al and Si in the as-prepared sample.

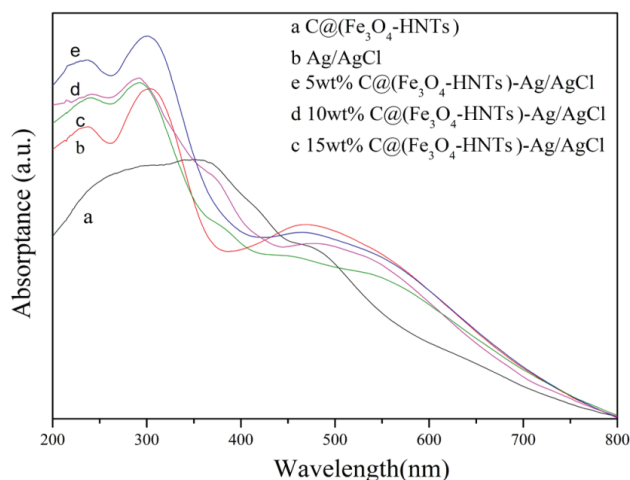


Fig. 4. UV-Vis absorption spectra of the composite photocatalyst with different C@(Fe<sub>3</sub>O<sub>4</sub>-HNT<sub>s</sub>) content.

Fig. 5(b) shows the high-resolution spectrum of O 1s. Fitting of the XPS O 1s spectra gives a detailed assignment of deconvoluted peaks. O 1s can be divided into four peaks, that is, the peak at 530.9, 532.2, 532.8 and 533.7 eV. The absorption peak at 530.9 eV is attributed to the binding energy of O element in carbonyl (C=O) group. The absorption peak at 532.2 eV is attributed to binding energy of O element in Si-O-Si chemical environment, and the binding energy of O element in the chemical environment of C-O-C is 532.8 eV. The binding energy at 533.7 eV is attributed to O element in -C-OH [34].

Fig. 5(c) shows high-resolution spectrum of Ag 3d, which exhibits two obvious peaks, corresponding to Ag 3d<sub>5/2</sub> and 3d<sub>3/2</sub> binding energies, respectively. Specifically, the two Ag 3d peaks can be further resolved into four peaks by the XPS peaks fitting program. The peaks at 374.9 and 368.7 eV originate from the metallic Ag species, and the 373.5 and 367.8 eV peaks are the Ag<sup>+</sup> iron, respectively [35].

In addition, the C1s spectra consist of four species (Fig. 5(d)). The absorption peak at 284.7 eV belongs to the binding energy of C element in -CH. The absorption peak at 286.08 eV is attributed to the binding energy of C elements in C-O and C=C. The absorption peak at 287.4 eV belongs to the binding energy of C elements in C=O and O-C-O. And, the peak at 289.2 eV is the absorption peak of carbon in O=C-O [36]. It can be shown that the carbon-containing functional groups are successfully grafted on the surface of composite Fe<sub>3</sub>O<sub>4</sub>-HNT<sub>s</sub>, which is consistent with the results given by the FTIR spectrum. Fe<sub>3</sub>O<sub>4</sub> and γ-Fe<sub>2</sub>O<sub>3</sub> have similar XRD patterns, Fe 2p binding energy of γ-Fe<sub>2</sub>O<sub>3</sub> is 719.0 eV, and the peak intensity at 719.0 eV is weaker due to divalent Fe in Fe<sub>3</sub>O<sub>4</sub> is on the surface of the particles, therefore, the Fe<sub>3</sub>O<sub>4</sub> nanomaterials are further confirmed by XPS [37].

The XPS spectra of Fe 2p of C@(Fe<sub>3</sub>O<sub>4</sub>-HNT<sub>s</sub>)-Ag/AgCl (Fig. 5(e)) showed peaks at 711.8 and 724.7 eV, which are the binding energies of Fe 2p<sub>3/2</sub> and Fe 2p<sub>1/2</sub> in Fe<sub>3</sub>O<sub>4</sub>, respectively, and were consistent with the values given by literature [38].

The Cl 2p spectrum in Fig. 5(f) displayed double peaks at 197.9 and 199.2 eV, which could be attributed to the binding energies of Cl 2p<sub>3/2</sub> and Cl 2p<sub>1/2</sub>, respectively [39].

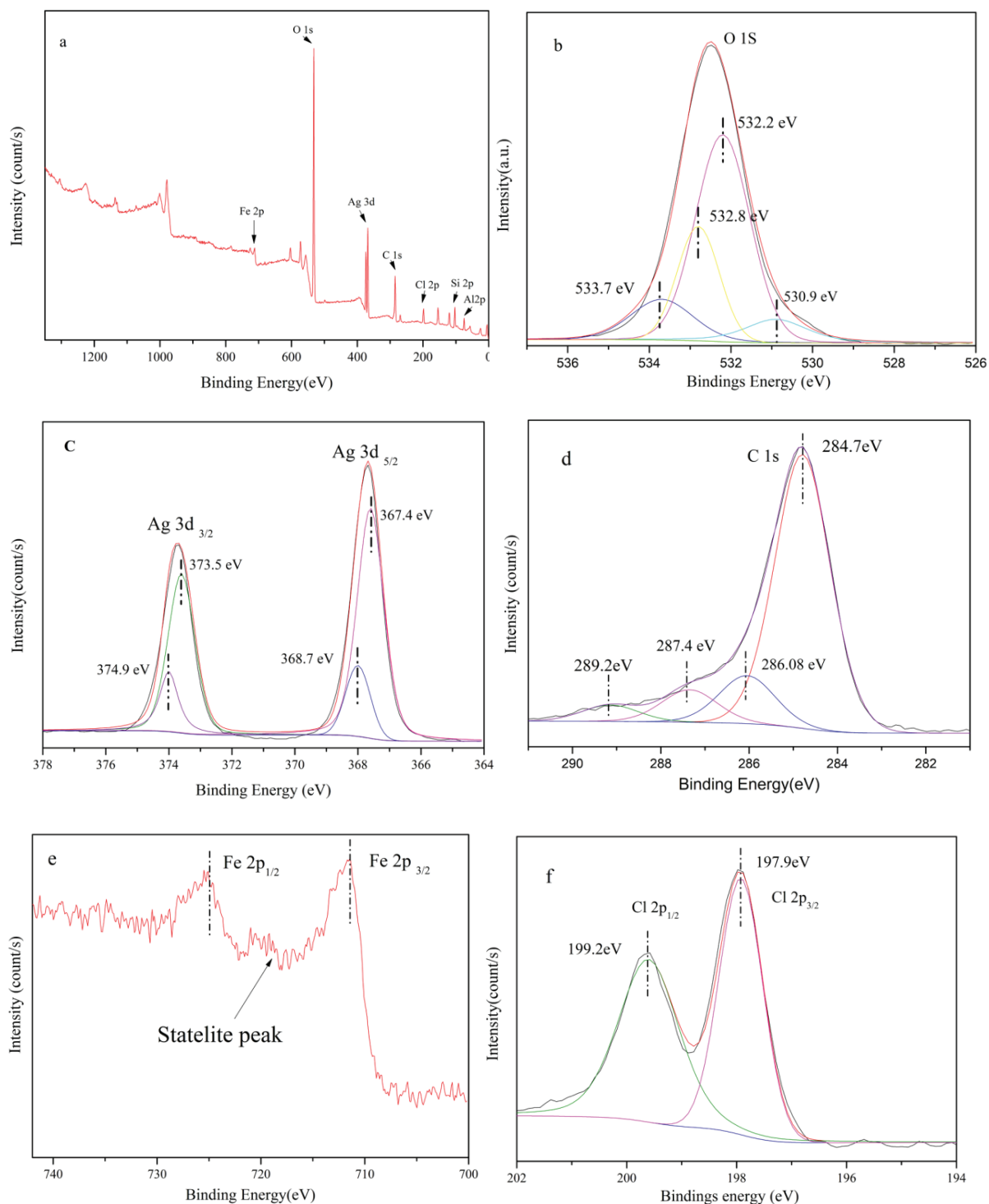


Fig. 5. XPS survey spectra of  $C@(\text{Fe}_3\text{O}_4\text{-HNT}_5)\text{-Ag/AgCl}$  (a) and high-resolution XPS spectra of O 1s (b), Ag 3d (c), C 1s (d), Fe 2p (e) and Cl 2p (f).

### 3.2. Photocatalytic degradation of methyl orange

The photocatalytic performance of Ag/AgCl,  $C@(\text{Fe}_3\text{O}_4\text{-HNT}_5)$  and  $C@(\text{Fe}_3\text{O}_4\text{-HNT}_5)\text{-Ag/AgCl}$  with different content of  $C@(\text{Fe}_3\text{O}_4\text{-HNT}_5)$  was evaluated by degradation of MO (10 mg/L) under visible-light irradiation ( $\lambda > 400$  nm).

The reaction of adsorption in the dark is also revealed in Fig. 6, all samples reach the adsorption equilibrium after 20 min.

As can be seen from Fig. 6, Ag/AgCl has no adsorption effect on MO, indicating that Ag/AgCl has very small specific surface area. With the cocatalyst  $C@(\text{Fe}_3\text{O}_4\text{-HNT}_5)$  content gradually increased, the adsorption efficiency of MO on to

the composite photocatalyst increased gradually in the dark adsorption stage due to adsorption of MO on to the carbonaceous functional groups and the HNT<sub>5</sub> with large specific surface area. For the composite photocatalyst with the best degradation performance, in which the cocatalyst C@(Fe<sub>3</sub>O<sub>4</sub>-HNT<sub>5</sub>) content is 5 wt%, the adsorption removal rate of MO was only 2.56%.

After 40 min of visible-light irradiation, the decolorization rates reached 83.68% for Ag/AgCl, while for 1 wt% C@(Fe<sub>3</sub>O<sub>4</sub>-HNT<sub>5</sub>)-Ag/AgCl, 5 wt% C@(Fe<sub>3</sub>O<sub>4</sub>-HNT<sub>5</sub>)-Ag/AgCl, 10 wt% C@(Fe<sub>3</sub>O<sub>4</sub>-HNT<sub>5</sub>)-Ag/AgCl and 15 wt% C@(Fe<sub>3</sub>O<sub>4</sub>-HNT<sub>5</sub>)-Ag/AgCl, reached 89.53%, 97.79%, 97.71% and 47.99%, respectively.

It can also be seen from Fig. 6 that C@(Fe<sub>3</sub>O<sub>4</sub>-HNT<sub>5</sub>) has no photocatalytic activity in itself, but its presence can accelerate the rate of photocatalytic reaction. This is because, first, the introduced HNT<sub>5</sub> could increase the specific surface areas of the composite photocatalyst; second, the carbonaceous functional groups and trivalent Fe on the surface of the C@(Fe<sub>3</sub>O<sub>4</sub>-HNT<sub>5</sub>) could capture the electrons produced by Ag/AgCl to make the electrons transferred to the surface of the supporter to hold back recombination of photogenerated electron and hole pair.

However, when the cocatalyst content reached 15 wt%, the function of C@(Fe<sub>3</sub>O<sub>4</sub>-HNT<sub>5</sub>) in the photocatalytic reaction could not compensate for the photocatalytic activity of the same amount of Ag/AgCl. So, the catalytic performance is poor.

### 3.3. Possible reaction mechanism

In order to identify the major active species in the process of photocatalytic degradation of MO, radical-trapping experiments were conducted by using three chemicals, that is, benzoquinone (a superoxide anion radical scavenger), disodium ethylenediaminetetraacetate (EDTA-2Na, a hole scavenger) and isopropyl alcohol (an OH· radical scavenger) [40]. The result is shown in Fig. 7.

The scavenger (10 mmol/L) was added to the MO solutions together with the photocatalyst prepared before the

visible-light irradiation. As depicted in Fig. 7, when EDTA-2Na and benzoquinone were added into the reaction liquid, the decolorization efficiency of MO was less than 20% after 60 min irradiation. Here, degradation of MO was due to the function of ·OH. However, when isopropyl alcohol was added into the reaction liquid, the decolorization efficiency of MO could reach 95.22%. These results indicate that ·O<sub>2</sub><sup>-</sup> and h<sup>+</sup> were the main active species in the photocatalytic reaction system. And, ·OH is also an active species in the system, but it plays a secondary role in the photocatalytic degradation.

At present research, via comparing the decoloration efficiency of MO by using C@(Fe<sub>3</sub>O<sub>4</sub>-HNT<sub>5</sub>)-Ag/AgCl with that by using (Fe<sub>3</sub>O<sub>4</sub>-HNT<sub>5</sub>)-Ag/AgCl, C@HNT<sub>5</sub>-Ag/AgCl, Fe<sub>3</sub>O<sub>4</sub>-Ag/AgCl and C@Fe<sub>3</sub>O<sub>4</sub>-Ag/AgCl, respectively, we can determine which part of the composites C@(Fe<sub>3</sub>O<sub>4</sub>-HNT<sub>5</sub>) plays a major role in the photocatalytic reaction. The results are shown in Fig. 8.

As can be seen from Fig. 8, the carbonaceous material and Fe<sub>3</sub>O<sub>4</sub> on the surface of C@(Fe<sub>3</sub>O<sub>4</sub>-HNT<sub>5</sub>) act as cocatalyst,

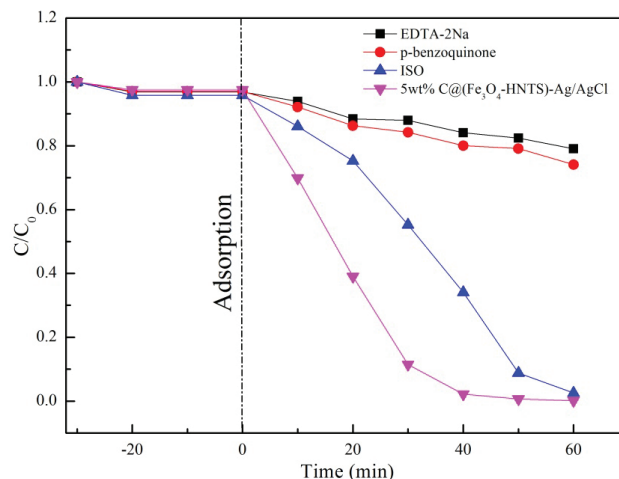


Fig. 7. Plots of active species trapping during photodegradation of MO by the as-obtained 5 wt% C@(Fe<sub>3</sub>O<sub>4</sub>-HNT<sub>5</sub>)-Ag/AgCl.

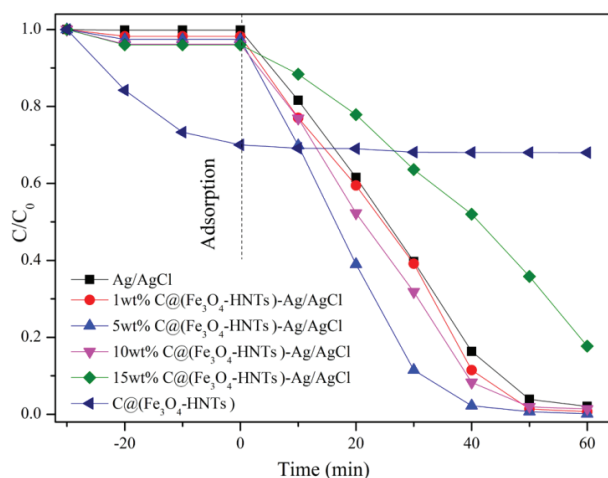


Fig. 6. Photodegradation of MO in the presence of different samples under visible-light irradiation.

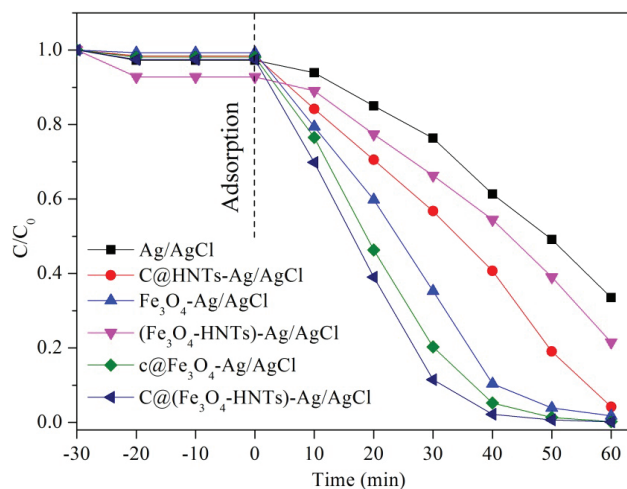


Fig. 8. Degradation of MO by Ag/AgCl embedding on various materials.

and in the presence of them, the degradation rate of MO by Ag/AgCl embedded on other materials is faster than that only by Ag/AgCl. Li et al. [13] prepared the nanocomposites  $\text{Fe}_3\text{O}_4/\text{TiO}_2/\text{Ag}$  and studied their photocatalytic properties. The results show that  $\text{Fe}_3\text{O}_4$  plays the role of a cocatalyst during catalytic reaction process, it not only transfers photogenerated carriers but also provides active sites for  $\text{O}_2$  to be reduced to  $\cdot\text{O}_2^-$ , thereby accelerating the photocatalytic reaction. Xu et al. [2] synthesized CNT/Ag/AgCl and found that the introduction of CNT can improve the photocatalytic reaction rate because CNT can not only increase the specific surface area of CNT/Ag/AgCl but also transfer photo-induced electrons. The results are consistent with those of this work. In other words, the separation of electron-hole pairs in the  $\text{C}@\text{(Fe}_3\text{O}_4\text{-HNTs)}\text{-Ag/AgCl}$  system would be more efficient than that in Ag/AgCl due to the presence of the cocatalyst  $\text{C}@\text{(Fe}_3\text{O}_4\text{-HNTs)}$ . To prove this suggestion, photoluminescence (PL) measurement was performed. Fig. 9 shows the PL testing curves of Ag/AgCl and 15 wt%  $\text{C}@\text{(Fe}_3\text{O}_4\text{-HNTs)}\text{-Ag/AgCl}$  composites. It is noteworthy that in this range the photocatalysts exhibit increasing emission intensity in the sequence: Ag/AgCl > 15 wt%  $\text{C}@\text{(Fe}_3\text{O}_4\text{-HNTs)}\text{-Ag/AgCl}$ . However, the activity of the photocatalysts declines in turns following the order: 15 wt%  $\text{C}@\text{(Fe}_3\text{O}_4\text{-HNTs)}\text{-Ag/AgCl}$  > Ag/AgCl. In general, the weaker PL emission intensity means the higher possibility of photogenerated carrier separation and hence the higher photocatalytic activity. Therefore, the PL spectra results suggest that high separation efficiency of the photogenerated carriers of 15 wt%  $\text{C}@\text{(Fe}_3\text{O}_4\text{-HNTs)}\text{-Ag/AgCl}$  might help improve its photocatalytic activity.

According to the results mentioned above, the possible reaction mechanism is illustrated in Fig. 10. When the composite catalyst  $\text{C}@\text{(Fe}_3\text{O}_4\text{-HNTs)}\text{-Ag/AgCl}$  was irradiated with visible light, the electron-hole pairs were generated due to the SPR [41], electron transferred to  $\text{Ag}^0$  nanoparticles far away from the surface of AgCl, while the holes transferred to the AgCl surface [42]. A part of electrons are trapped by  $\text{O}_2$  in the solution to form  $\cdot\text{O}_2^-$  and the other electrons migrate to the surface of the cocatalyst by carbonaceous functional

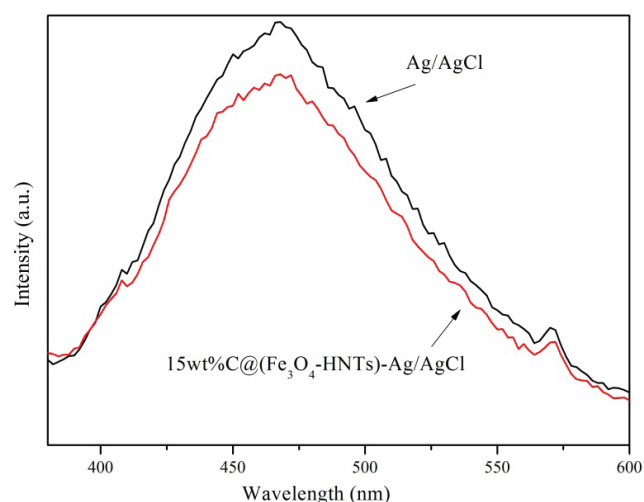


Fig. 9. Photoluminescence spectra of Ag/AgCl and 15 wt%  $\text{C}@\text{(Fe}_3\text{O}_4\text{-HNTs)}\text{-Ag/AgCl}$  with excitation at 470 nm.

groups' trapping, and the electrons are trapped by  $\text{O}_2$  to form  $\cdot\text{O}_2^-$ . Furthermore,  $\cdot\text{O}_2^-$  participate in degradation of MO. The holes as another active group were captured by  $\text{OH}^-$  to generate  $\cdot\text{OH}$  free radicals in the solution or directly involved in degradation of MO by binding with  $\text{Cl}^-$  to form  $\text{Cl}^0$  atoms.  $\text{Cl}^0$  atoms and  $\cdot\text{OH}$  free radicals were reduced back to  $\text{Cl}^-$  and  $\text{OH}^-$ , respectively, after receiving the electrons from MO.

### 3.4. Recycled performances

5 wt%  $\text{C}@\text{(Fe}_3\text{O}_4\text{-HNTs)}\text{-Ag/AgCl}$  was used repeatedly to degrade MO to evaluate its photocatalytic stabilities without new catalyst. After reaction in each run (60 min), the photocatalyst was collected by centrifugation and dried by oven for the next use. The photocatalyst was recycled for five times. The results are shown in Fig. 11.

As can be seen from Fig. 11, the photocatalytic degradation efficiency of MO decreased from 99.29% to 91.2% after five cycles of 5 wt%  $\text{C}@\text{(Fe}_3\text{O}_4\text{-HNTs)}\text{-Ag/AgCl}$ . The slight activity decline could be attributed to washout loss of some photocatalyst during recovery steps and the deposition of reaction products on the catalyst surface [43]. Another possible reason is the photocorrosion of a part of Ag/AgCl during the reaction process. The third possible reason is that the dispersibility of the photocatalyst became worse compared with the initial use in the process of recycling [44]. These results (Fig. 11) indicate that the stability of  $\text{C}@\text{(Fe}_3\text{O}_4\text{-HNTs)}\text{-Ag/AgCl}$  is good and the catalyst can be reused. The growth of Ag/AgCl on the surface of  $\text{C}@\text{(Fe}_3\text{O}_4\text{-HNTs)}$  can improve the visible light photocatalytic performance of Ag/AgCl and inhibit the photocorrosion, resulting in a stable durability of photocatalytic activity.

Wang et al. [45] proposed the catalytic mechanism of Ag/AgCl that the Ag nanoclusters on the surface of AgCl are the main materials for absorbing photons, and an absorbed photon would be efficiently separated into an electron and a hole, so that the electron on  $\text{Ag}^0$  nanoclusters is transferred

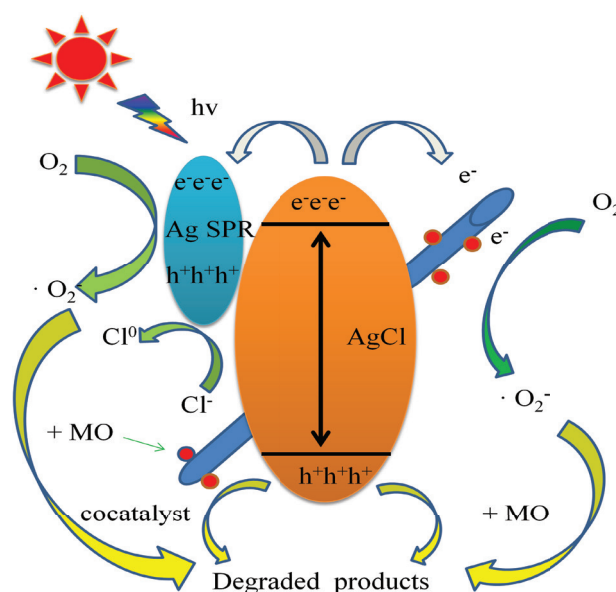


Fig. 10. Schematic photocatalytic reaction process and charge transfer of  $\text{C}@\text{(Fe}_3\text{O}_4\text{-HNTs)}\text{-Ag/AgCl}$  on MO removal.

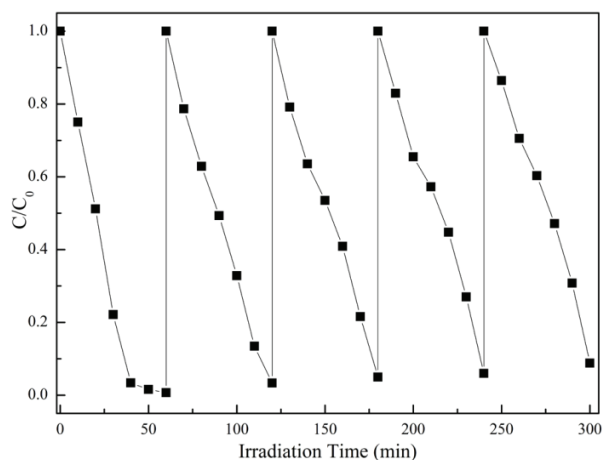


Fig. 11. Cycling experiment of photocatalytic degradation of MO by 5 wt% C@(Fe<sub>3</sub>O<sub>4</sub>-HNT<sub>s</sub>)-Ag/AgCl under visible-light irradiation (initial concentration of MO solution is 10 mg/L, solution volume is 100 mL, dosage of 5 wt% C@(Fe<sub>3</sub>O<sub>4</sub>-HNT<sub>s</sub>)-Ag/AgCl is 500 mg/L).

to another surface farthest away from the Ag/AgCl; e<sup>-</sup> is captured by O<sub>2</sub> in solution to generate ·O<sub>2</sub><sup>-</sup>, and the hole (h<sup>+</sup>) transferred to the surface of the AgCl particle, Cl<sup>-</sup> was reduced to Cl<sup>0</sup>, as chlorine atoms are reactive radical species, they should be able to directly oxidize MO and hence be reduced to chloride ions again [12], or the holes of catalyst react with some OH<sup>-</sup> or H<sub>2</sub>O molecules to form hydroxyl radicals (·OH), which can further participate in photocatalytic reaction. The reason for the high stability of Ag/AgCl and C@(Fe<sub>3</sub>O<sub>4</sub>-HNT<sub>s</sub>)-Ag/AgCl is that the photons are absorbed by Ag nanoclusters, a small fraction of the electrons separated from the absorbed photons continued to locate at the end of the Ag nanocluster away from the AgCl, and most of the electrons were captured by C@(Fe<sub>3</sub>O<sub>4</sub>-HNT<sub>s</sub>), not were transferred to Ag<sup>+</sup> ions of the AgCl lattice. Therefore, under visible light irradiation, C@(Fe<sub>3</sub>O<sub>4</sub>-HNT<sub>s</sub>) may carrier transfer rapidly and photocorrosion will be inhibited. Thus the composite photocatalyst C@(Fe<sub>3</sub>O<sub>4</sub>-HNT<sub>s</sub>)-Ag/AgCl showed high stability and strong catalytic performance.

#### 4. Conclusions

Plasma photocatalyst C@(Fe<sub>3</sub>O<sub>4</sub>-HNT<sub>s</sub>)-Ag/AgCl was synthesized successfully via the three-step method. The composite photocatalyst containing 5 wt% of C@(Fe<sub>3</sub>O<sub>4</sub>-HNT<sub>s</sub>) has a strong light response in ultraviolet and visible regions (400–800 nm). The photo-degradation efficiency of MO by using 5 wt% C@(Fe<sub>3</sub>O<sub>4</sub>-HNT<sub>s</sub>)-Ag/AgCl reached to 97.79% after 40 min of visible light irradiation.

In the photocatalytic reaction system, the active oxidative species ·O<sub>2</sub><sup>-</sup> and h<sup>+</sup> contributed most to the decolorization reaction of MO, ·OH is a less important reactive group, which also plays a certain role in degradation. The carbonaceous material on the surface of composite C@(Fe<sub>3</sub>O<sub>4</sub>-HNT<sub>s</sub>) and Fe<sub>3</sub>O<sub>4</sub> plays the role of cocatalyst. The photocatalytic degradation reaction rate of MO has been significantly increased because of the presence of the carbonaceous material and Fe<sub>3</sub>O<sub>4</sub>.

The as-prepared composite plasma photocatalyst C@(Fe<sub>3</sub>O<sub>4</sub>-HNT<sub>s</sub>)-Ag/AgCl not only has strong photocatalytic activity under visible-light irradiation but also has good reusability, and has potential application in photodegradation of azo dyes.

#### Acknowledgment

This work was supported by Zhangjiagang Science and Technology Support Program (Social Development) of Jiangsu Province, China (grant numbers: ZKS1510).

#### References

- [1] Q. Zhang, Y. Zhou, Z. Zhang, Y. He, Y.D. Chen, Y.H. Lin, Plasmonic photocatalyst, *Prog. Chem.*, 25 (2013) 2020–2027.
- [2] Y.G. Xu, M. Xie, T. Zhou, S. Yin, H. Xu, H.Y. Ji, H.M. Li, Q. Zhang, In situ growth of Ag/AgCl on the surface of CNT and the effect of CNT on the photoactivity of the composite, *New J. Chem.*, 39 (2015) 5540–5547.
- [3] Z.W. Liu, W.B. Hou, P. Pavaskar, M. Aykol, S.B. Cronin, Plasmon resonant enhancement of photocatalytic water splitting under visible illumination, *Nano Lett.*, 11 (2011) 1111–1116.
- [4] C.J. Miller, H.J. Yu, T.D. Waite, Degradation of rhodamine B during visible light photocatalysis employing Ag@AgCl embedded on reduced graphene oxide, *Colloids Surf., A*, 435 (2013) 147–153.
- [5] H.J. Yu, C.J. Miller, A. Ikeda-Ohno, T.D. Waite, Photodegradation of contaminants using Ag@AgCl/rGO assemblages: possibilities and limitations, *Catal. Today*, 224 (2014) 122–131.
- [6] L. Zhou, H.Y. Zhang, H.Q. Sun, S.M. Liu, M.O. Tade, S.B. Wang, W.Q. Jin, Recent advances in non-metal modification of graphitic carbon nitride for photocatalysis: a historic review, *Catal. Sci. Technol.*, 6 (2016) 7002–7023.
- [7] J. Tian, R. Liu, G.H. Wang, Y. Xu, X.F. Wang, H.G. Yu, Dependence of metallic Ag on the photocatalytic activity and photoinduced stability of Ag/AgCl photocatalyst, *Appl. Surf. Sci.*, 319 (2014) 324–331.
- [8] X.J. Wen, C.G. Niu, L. Zhang, D.W. Huang, G.M. Zeng, In-situ synthesis of visible-light-driven plasmonic Ag/AgCl-CdWO<sub>4</sub> photocatalyst, *Ceram. Int.*, 43 (2017) 1922–1929.
- [9] S. Garg, H.Y. Rong, C.J. Miller, T.D. Waite, Chlorine-mediated regeneration of semiconducting AgCl(s) following light-induced Ag<sup>0</sup> formation: implications to contaminant degradation, *J. Phys. Chem. C*, 120 (2016) 5988–5996.
- [10] M. Cargnello, T. Montini, S.Y. Smolin, J.B. Priebe, J.J. Delgado, V.V. Doan-Nguyen, I.S. McKay, J.A. Schwalbe, M.M. Pohl, T.R. Gordon, Y.P. Lu, J.B. Baxter, A. Brückner, P. Fornasiero, C.B. Murray, Engineering titania nanostructure to tune and improve its photocatalytic activity, *Proc. Natl. Acad. Sci. USA*, 113 (2016) 3966–3971.
- [11] Z.F. Zhao, Y.Z. Wang, J. Xu, Y. Wang, Mesoporous Ag/TiO<sub>2</sub> nanocomposites with greatly enhanced photocatalytic performance towards degradation of methyl orange under visible light, *RSC Adv.*, 5 (2015) 59297–59305.
- [12] L. Liu, S.L. Lin, J.S. Hu, Y.H. Liang, W.Q. Cui, Growth of nano Ag@AgCl on (111) facets of Cu<sub>2</sub>O microcrystals with an enhanced photocatalytic activity, *RSC Adv.*, 5 (2015) 62306–62313.
- [13] T.T. Li, Y.M. He, H.J. Lin, J. Cai, L.Z. Dong, X.X. Wang, M.F. Luo, L.H. Zhao, X.D. Yi, W.Z. Weng, Synthesis, characterization and photocatalytic activity of visible-light plasmonic photocatalyst AgBr-SmVO<sub>4</sub>, *Appl. Catal., B*, 138–139 (2013) 95–103.
- [14] L.Z. Dong, Y.M. He, T.T. Li, J. Cai, W.D. Hu, S.S. Wang, H.J. Lin, M.F. Luo, X.D. Yi, L.H. Zhao, W.Z. Weng, H.L. Wan, A comparative study on the photocatalytic activities of two visible-light plasmonic photocatalysts: AgCl-SmVO<sub>4</sub> and AgI-SmVO<sub>4</sub> composites, *Appl. Catal., A*, 472 (2014) 143–151.
- [15] Y.L. Zhao, C.R. Tao, G. Xiao, G.P. Wei, L.H. Li, C.X. Liu, H.J. Su, Controlled synthesis and photocatalysis of sea urchin-like Fe<sub>3</sub>O<sub>4</sub>@TiO<sub>2</sub>@Ag nanocomposites, *Nanoscale*, 8 (2016) 5313–5326.

- [16] Y.G. Xu, H. Xu, H.M. Li, J.X. Xia, C.T. Liu, L. Liu, Enhanced photocatalytic activity of new photocatalyst Ag/AgCl/ZnO, *J. Alloys Compd.*, 509 (2011) 3286–3292.
- [17] X.X. Yao, X. Liu, One-pot synthesis of Ag/AgCl@SiO<sub>2</sub> core-shell plasmonic photocatalyst in natural geothermal water for efficient photocatalysis under visible light, *J. Mol. Catal. A Chem.*, 393 (2014) 30–38.
- [18] X.P. Wang, T.T. Lim, Highly efficient and stable Ag–AgBr/TiO<sub>2</sub> composites for destruction of *Escherichia coli* under visible light irradiation, *Water Res.*, 47 (2013) 4148–4158.
- [19] M. Cui, J.X. Yu, H.J. Lin, Y. Wu, L.H. Zhao, Y.M. He, In-situ preparation of Z-scheme AgI/Bi<sub>2</sub>O<sub>3</sub> hybrid and its excellent photocatalytic activity, *Appl. Surf. Sci.*, 387 (2016) 912–920.
- [20] J.X. Yu, M. Cui, X.Z. Liu, Q.Q. Chen, Y. Wu, Y.M. He, Preparation of novel AgBr/Bi<sub>2</sub>O<sub>3</sub> hybrid with high photocatalytic activity via in situ ion exchange method, *Mater. Lett.*, 193 (2017) 73–76.
- [21] X.N. He, F. Su, Z.Z. Lou, W.Z. Jia, Y.L. Song, H.Y. Chang, Y.H. Wu, J. Lan, X.Y. He, Y. Zhang, Ipr1 gene mediates RAW 264.7 macrophage cell line resistance to *Mycobacterium bovis*, *Scand. J. Immunol.*, 74 (2011) 438–444.
- [22] L.M. Song, J.F. Yang, S.J. Zhang, Enhanced photocatalytic activity of Ag<sub>3</sub>PO<sub>4</sub> photocatalyst via glucose-based carbonsphere modification, *Chem. Eng. J.*, 309 (2016) 222–229.
- [23] Y.H. Liang, S.L. Lin, L. Liu, J.S. Hu, W.Q. Cui, Oil-in-water self-assembled Ag@AgCl QDs sensitized Bi<sub>2</sub>WO<sub>6</sub>: enhanced photocatalytic degradation under visible light irradiation, *Appl. Catal., B*, 164 (2015) 192–203.
- [24] W.Q. Cui, H. Wang, Y.H. Liang, B.X. Han, L. Liu, J.S. Hu, Microwave-assisted synthesis of Ag@AgBr-intercalated K<sub>4</sub>Nb<sub>6</sub>O<sub>17</sub> composite and enhanced photocatalytic degradation of Rhodamine B under visible light, *Chem. Eng. J.*, 230 (2013) 10–18.
- [25] J. Liu, G.K. Zhang, Recent advances in synthesis and applications of clay-based photocatalysts: a review, *Phys. Chem. Chem. Phys.*, 16 (2014) 8178–8192.
- [26] T.Y. Xu, R.L. Zhu, J.X. Zhu, X.L. Liang, Y. Liu, Y. Xu, H.P. He, Ag<sub>3</sub>PO<sub>4</sub> immobilized on hydroxy-metal pillared montmorillonite for the visible light driven degradation of acid red 18, *Catal. Sci. Technol.*, 6 (2016) 4116–4123.
- [27] S.T. Zhong, W. Jiang, M. Han, G.Z. Liu, N. Zhang, Y. Lu, Graphene supported silver@silver chloride & ferrous oxide hybrid, a magnetically separable photocatalyst with high performance under visible light irradiation, *Appl. Surf. Sci.*, 347 (2015) 242–249.
- [28] X.P. Wu, W.Y. Zhu, X.L. Zhang, T.H. Chen, R. Frost, Catalytic deposition of nanocarbon onto palygorskite and its adsorption of phenol, *Appl. Clay Sci.*, 52 (2011) 400–406.
- [29] X. Tian, W. Wang, N. Tian, C. Zhou, C. Yang, S. Komarneni, Cr(VI) reduction and immobilization by novel carbonaceous modified magnetic Fe<sub>3</sub>O<sub>4</sub>/halloysite nanohybrid, *J. Hazard. Mater.*, 309 (2016) 151–156.
- [30] J. Jin, L.J. Fu, H.M. Yang, J. Ouyang, Carbon hybridized halloysite nanotubes for high-performance hydrogen storage capacities, *Sci. Rep.*, 5 (2015) 12429–12438.
- [31] H.S. Kambo, A. Dutta, A comparative review of biochar and hydrochar in terms of production, physico-chemical properties and applications, *Renew. Sust. Energy Rev.*, 45 (2015) 359–378.
- [32] X.F. Cao, X.W. Peng, S.N. Sun, L.X. Zhong, W. Chen, S. Wang, R.C. Sun, Hydrothermal conversion of xylose, glucose, and cellulose under the catalysis of transition metal sulfates, *Carbohydr. Polym.*, 118 (2015) 44–51.
- [33] Z.Z. Lou, Z.Y. Wang, B.B. Huang, Y. Dai, Synthesis and activity of plasmonic photocatalysts, *ChemCatChem*, 6 (2014) 2456–2476.
- [34] Y.J. Xu, G. Weinberg, X. Liu, O. Timpe, R. Schlogl, D.S. Su, Nanoarchitecturing of activated carbon: facile strategy for chemical functionalization of the surface of activated carbon, *Adv. Funct. Mater.*, 18 (2008) 3613–3619.
- [35] H.Y. Li, Y.J. Sun, B. Cai, S.Y. Gan, D.X. Han, L. Niu, T.S. Wu, Hierarchically Z-scheme photocatalyst of Ag@AgCl decorated on BiVO<sub>4</sub> (0 4 0) with enhancing photoelectrochemical and photocatalytic performance, *Appl. Catal., B*, 170–171 (2015) 206–214.
- [36] Z.R. Yue, S.E. Bender, J.W. Wang, J. Economy, Removal of chromium Cr(VI) by low-cost chemically activated carbon materials from water, *J. Hazard. Mater.*, 166 (2009) 74–78.
- [37] X. Teng, D. Black, N.J. Watkins, Y. Gao, H. Yang, Platinum-maghemite core-shell nanoparticles using a sequential synthesis, *Nano Lett.*, 3 (2003) 261–264.
- [38] Y. Tian, B.B. Yu, X. Li, K. Li, Facile solvothermal synthesis of monodisperse Fe<sub>3</sub>O<sub>4</sub> nanocrystals with precise size control of one nanometre as potential MRI contrast agents, *J. Mater. Chem.*, 21 (2011) 2476–2481.
- [39] B.Y. Wang, M. Zhang, W.Z. Li, L.L. Wang, J. Zheng, W.J. Gan, J.L. Xu, Fabrication of Au(Ag)/AgCl/Fe<sub>3</sub>O<sub>4</sub>@PDA@Au nanocomposites with enhanced visible-light-driven photocatalytic activity, *Dalton Trans.*, 44 (2015) 17020–17025.
- [40] J.T. Tang, Y.H. Liu, H.Z. Li, Z. Tan, D.T. Li, A novel Ag<sub>3</sub>AsO<sub>4</sub> visible-light-responsive photocatalyst: facile synthesis and exceptional photocatalytic performance, *Chem. Commun.*, 49 (2013) 5498–5500.
- [41] J.G. Yu, G.P. Dai, B.B. Huang, Fabrication and characterization of visible-light-driven plasmonic photocatalyst Ag/AgCl/TiO<sub>2</sub> nanotube arrays, *J. Phys. Chem. C*, 113 (2009) 16394–16401.
- [42] M.S. Zhu, P.L. Chen, M.H. Liu, Graphene Oxide Enwrapped Ag/AgX (X = Br, Cl) nanocomposite as a highly efficient visible-light plasmonic photocatalyst, *ACS Nano*, 5 (2011) 4529–4536.
- [43] C. McManamon, J.D. Holmes, M.A. Morris, Improved photocatalytic degradation rates of phenol achieved using novel porous ZrO<sub>2</sub>-doped TiO<sub>2</sub> nanoparticulate powders, *J. Hazard. Mater.*, 193 (2011) 120–127.
- [44] A.G. Zhigotskii, E.F. Rynda, N.A. Mishchuk, V.M. Kochkodan, A.V. Ragulya, V.P. Klimenko, M.N. Zagornyi, A study of the photocatalytic activity of titanium dioxide nanopowders, *Russ. J. Appl. Chem.*, 81 (2008) 2056–2061.
- [45] P. Wang, B.B. Huang, X.Y. Qin, X.Y. Zhang, Y. Dai, J.Y. Wei, M.H. Whangbo, Ag@AgCl: a highly efficient and stable photocatalyst active under visible light, *Angew. Chem.*, 47 (2008) 7931–7933.